catalysts

MDPI

Article

Waste for Product: Pd and Pt Nanoparticle-Modified Ni Foam as a Universal Catalyst for Hydrogen/Oxygen Evolution Reaction and Methyl Orange Degradation

Julia Druciarek, Dawid Kutyła, Adrianna Pach, Anna Kula and Magdalena Luty-Błocho *

AGH University of Krakow, Faculty of Non-Ferrous Metals, Al. A. Mickiewicza 30, 30-059 Krakow, Poland; jdruciarek@student.agh.edu.pl (J.D.); kutyla@agh.edu.pl (D.K.); apach@agh.edu.pl (A.P.); kula@agh.edu.pl (A.K.)
* Correspondence: mlb@agh.edu.pl

Abstract: Declining natural resources make the recovery of metals from waste solutions a promising alternative. Moreover, processing waste into a finished product has its economic justification and benefits. Thus, the aim of this research was developing a Waste for Product strategy, indicating the possibility of processing solutions with a low content of platinum-group metals for catalyst synthesis. The results obtained confirmed that diluted synthetic waste solutions containing trace amount of valuable metal ions (Pd, Pt) can be used for the process of catalyst synthesis. Catalysts produced in the form of palladium and platinum nanoparticles were successfully deposited on a Ni foam due to the galvanic displacement mechanism. Synthesized catalysts were characterized using UV-Vis spectrophotometry, SEM/EDS, and XRD techniques. Electro- and catalytic properties were tested for hydrogen/oxygen evolution reactions and methyl orange degradation, respectively. The results obtained from electrocatalytic tests indicated that the modification of the nickel foam surface by waste solutions consisting of noble metals ions as Pd and Pt can significantly increase the activity in hydrogen and oxygen evolution reactions in comparison to non-treated samples. Catalytic tests performed for the process of methyl orange degradation shorten the time of the process from several hours to 15 min. The most favorable results were obtained for the catalysts in the following order Pd1.0Pt0@Ni > Pd0Pt1.0@Ni > Pd0.5Pt0.5@Ni > Ni foam > no catalyst, indicating the best catalytic performance for catalyst containing pure palladium nanoparticles deposited on the nickel surface.

Keywords: catalyst; Ni foam; PtNPs; PdNPs; HER; OER; azo dyes degradation; methyl orange; H_2O_2

Academic Editors: Detlef W. Bahnemann, Yaron Paz and Maria G. Antoniou

Received: 31 October 2024
Revised: 23 January 2025
Accepted: 27 January 2025
Published: 30 January 2025

Citation: Druciarek, J.; Kutyła, D.; Pach, A.; Kula, A.; Luty-Błocho, M. Waste for Product: Pd and Pt Nanoparticle-Modified Ni Foam as a Universal Catalyst for Hydrogen/Oxygen Evolution Reaction and Methyl Orange Degradation. *Catalysts* **2025**, *15*, 133. https://doi.org/10.3390/catal15020133

1. Introduction

Platinum-group metals (PGMs) are important elements that are widely used in various fields, particularly in catalysis. These metals are distinguished by high chemical resistance and catalytic activity in processes such as hydrogen evolution, synthesis of organic compounds, performance of fuel cells, etc. Platinum's optimal hydrogen adsorption energy allows it to act as one of the most effective electrocatalysts [1–5]. Platinum plays a crucial role in the oxidation of hydrogen at the anode and the reduction of oxygen at the cathode, significantly contributing to energy conversion efficiency in fuel cells [6–8]. For catalytic purposes, it is also often used in combination with other metals [9] as a platinum-based bimetallic catalyst [10] to increase reaction efficiency and/or reduce costs.

Palladium is another critical metal in catalysis, especially in organic synthesis. It is extensively used in carbon–carbon bond formation reactions, such as Suzuki, Heck, and

Sonogashira couplings, which are vital for the production of pharmaceuticals and fine chemicals [11–15]. Shrinking natural resources mean that methods for recovering valuable metals from post-production solutions have already been developed for a long time. However, a low concentration of valuable metals in waste solutions makes problematic the application of existing methods for their efficient recovery like extraction, precipitation, etc. [16]. These methods are efficient but are limited by specific process conditions and require expensive reagents [17]. Moreover, the extraction requires an additional process which releases extracted metals and allows for their accumulation. For a highly diluted solution containing precious metals, the adsorption process can be used. However, there is the negative impact of an absorber related to its low selectivity. For example, carbon-based materials can absorb both organic and inorganic compounds. Only a modulation of surface groups and environmental conditions might improve their selectivity. Another problem results from PGMs' negative impact on the environment. Heavy metals accumulate in living organisms, leading to various diseases [18–20]. There is also a need to solve the problem of metals recovery from various environments. Recently, the Waste for Product (W4P) strategy was proposed by our group as a promising tool for transferring metal ions from a waste solution directly to a ready-to-use product. We showed that it is possible to make a bimetallic electrocatalyst deposited on activated carbon fibers in a microreactor system [21], or even palladium nanopyramids enriched with platinum nanoparticles deposited on activated carbon [22]. In both cases, we used a highly diluted mixture of the aqueous solution containing Pt(IV) and Pd(II) ions and mild acidic conditions. In this work, we continue our activity related to the development of the W4P strategy. Unlike previous work, we decided to replace the catalytic carbon carrier with a nickel foam for two key reasons. First, we aim to explore alternative catalytic supports beyond carbon. Activated carbon, while effective in capturing valuable metals, unfortunately also adsorbs various inorganic and organic compounds, which may pose challenges for practical applications in industrial solutions. Ultimately, the presence of other species on the catalytic carrier may negatively affect its performance. Second, we wanted to investigate whether enriching the nickel foam with a thin nano-layer of platinum-group metals will have a positive effect on the catalyzed reaction. For example, Yang et al. showed the ability of a unique Pt-O-Ni bridge constructed between platinum nanoparticles and nickel metaphosphate to change the coordination and electronic environment. The synthesized material shows long-term stability and operates over a wide pH range [23].

This research is aimed at the development of a multifunctional catalyst for both hydrogen/oxygen evolution reactions and azo dye degradation. We considered two primary catalyst types: an unmodified Ni foam and Ni foam modified by a galvanic displacement process with a solution consisting of different PGM amounts (catalysts composition: Pd1.0Pt0@Ni, Pd0.75Pt0.25@Ni, Pd0.5Pt0.5@Ni, Pd0.25Pt0.74@Ni, Pd0Pt1.0@Ni) to study their electrocatalytic effect on hydrogen/oxygen evolution reactions. For the methyl orange degradation process, we selected the following catalysts: Pd1.0Pt0@Ni, Pd0.5Pt0.5@Ni, and Pd0Pt1.0@Ni. Commercially available Ni foam was modified by impregnation in a solution containing PGM ions in the batch reactor after chemical treatment. The process was carried out at constant temperature and mixing rate, and with different metal ion compositions, but at a low concentration typical for waste solution. In the resulting galvanic displacement between Ni and PGM, we obtained catalysts with different composition, morphology, and catalytic properties.

2. Results and Discussion

2.1. Spectra of Reagents

Before Ni foam modification, all solutions containing metal ions and their mixture (see, Supplementary Materials (Table S1) for details) were analyzed using UV-Vis spectrophotometry. Obtained spectra are shown in Figure 1.

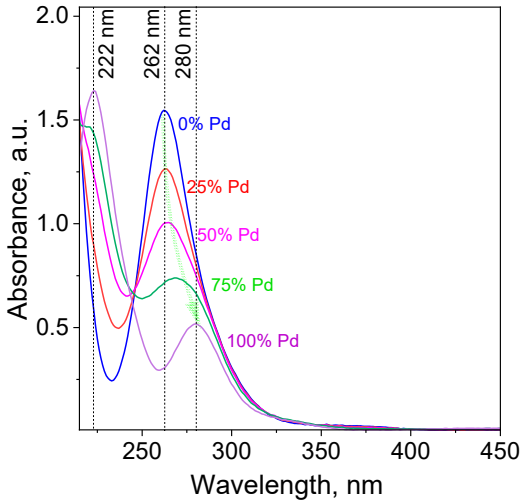

Figure 1. The spectra of the solution containing metal ions for Ni foam modification. Conditions: $C_{0,Pd(II)}$ = 5 × 10^{-5} M (100% Pd, 0% Pt in the solution), $C_{0,Pd(II)}$ = 0.375 × 10^{-5} M and $C_{0,Pt(IV)}$ = 0.125 × 10^{-5} M (75% Pd, 25% Pt in the solution), $C_{0,Pd(II)}$ = 0.25 × 10^{-5} M and $C_{0,Pt(IV)}$ = 0.25 × 10^{-5} M (50% Pd, 50% Pt in the solution), $C_{0,Pd(II)}$ = 0.125 × 10^{-5} M and $C_{0,Pt(IV)}$ = 0.375 × 10^{-5} M (25% Pd, 75% Pt in the solution), $C_{0,Pt(IV)}$ = 1 × 10^{-5} M (0% Pd, 100% Pt in the solution), 0.1 M HCl solution as solvent, T = 20 °C.

The spectrum registered for the solution containing Pd(II) ions has characteristic maxima at 222 and 280 nm (100% Pd, Figure 1). According to the literature [24], these peaks are assigned to the $[PdCl_4]^{2-}$ complex. The solution containing Pt(IV) ions in the considered concentration range has a characteristic peak at 262 nm (0% Pd, Figure 1). The location of this maximum is typical for $[PtCl_6]^{2-}$ and $[PtCl_5(H_2O)]^{-}$ complexes [25]. Considering the applied 0.1 M HCl solution as the solvent (which suppresses the hydrolysis process), we have only $[PtCl_6]^{2-}$ complex in the solution. A mixture of Pd(II) and Pt(IV) ions provides the final spectrum, with maximum red shift (green arrow, Figure 1) (observed change in peak position from 262 to 268 nm for solutions 25% Pd and 75% Pd, respectively). A changing share between Pd(II) and Pt(IV) ions produces spectra with less intensity (see, Figure 1) and it is the total spectrum derived from the individual spectra of both metal ions. Registered spectra are used for tracking amount of these ions in the solution during the galvanic displacement process.

2.2. Synthesis of Catalyst with Different Composition

The Ni foam modification was carried out in a batch reactor containing different solutions (see, Supplementary Materials, Table S1), at a constant mixing rate (1000 rpm, magnetic bar with diameter 0.5 cm and 1 cm long), volume (4 mL), and temperature (20 °C). The process was carried out for an optimal duration of 5 min to achieve a thin layer of platinum and palladium on the Ni foam surface. Extending the time led to an excessively thick metal layer, which adversely impacted the catalytic process, as the metal layer tended to detach from the foam surface.

Immersing the nickel foam in the solution containing noble metal ions spontaneously initiates the reaction, known as a galvanic displacement. Considering the electrochem-

ical series, Ni belongs to the non-noble metals with the value of standard potential $E^{\circ} = -0.23$ V. Contrary to nickel, palladium and platinum belong to the noble metals with standard potential values under experimental conditions (chloride 0.1 M, pH = 1) of $E^{\circ}_{Pd(II)/Pd} = 0.591$ V and $E^{\circ}_{Pt(IV)/Pt} = 0.68$ V, respectively. Thus, Ni in a zero oxidation state and noble metal ions create an ideal system for single exchange reaction. In this reaction, more noble metal ions are reduced to the metal in a zero oxidation state, whereas nickel is oxidized to Ni(II), as per Equations (1) and (2).

$$Ni + Pd(II) \rightarrow Ni(II) + Pd \quad (1)$$

$$2Ni + Pt(IV) \rightarrow 2Ni(II) + Pt \quad (2)$$

The progress of these reactions (1) and (2) was monitored spectrophotemetrically. Depending on the solution composition, a change in the absorbance at different wavelengths (λ_{max}: 262 nm for 0% Pd, 25% Pd; 263 nm for 50% Pd; 268 nm for 75% Pd and 280 nm for 100% Pd) was registered. After 5 min, the process was stopped, and the Ni foam was isolated from the solution. Next, the obtained catalyst was rinsed with deionized water and ethanol and set to dry for 20 min at 70 °C. The solution was then analyzed spectrophotometrically, with the result presented in Figure 2.

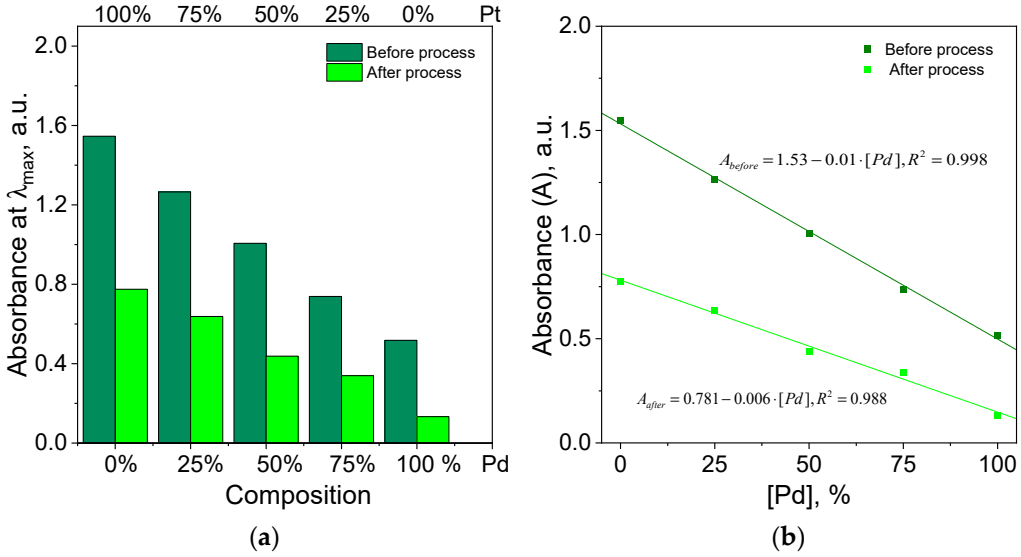

Figure 2. The values of the absorbance registered at λ_{max} characteristic for each solution composition (λ_{max}: 262 nm for 0% Pd, 25% Pd; 263 nm for 50% Pd; 268 nm for 75% Pd, and 280 nm for 100% Pd) before and after process of Ni foam impregnation (**a**); dependence of absorbance as a function of palladium ion concentration (**b**). Conditions: $C_{0,Pd(II)} = 5 \times 10^{-5}$ M (100% Pd, 0% Pt in the solution), $C_{0,Pd(II)} = 0.375 \times 10^{-5}$ M and $C_{0,Pt(IV)} = 0.125 \times 10^{-5}$ M (75% Pd, 25% Pt in the solution), $C_{0,Pd(II)} = 0.25 \times 10^{-5}$ M and $C_{0,Pt(IV)} = 0.25 \times 10^{-5}$ M (50% Pd, 50% Pt in the solution), $C_{0,Pd(II)} = 0.125 \times 10^{-5}$ M and $C_{0,Pt(IV)} = 0.375 \times 10^{-5}$ M (25% Pd, 75% Pt in the solution), $C_{0,Pt(IV)} = 1 \times 10^{-5}$ M (0% Pd, 100% Pt in the solution), 0.1 M HCl solution as solvent, T = 20 °C.

In each case, a decrease in the absorbance value roughly by half was observed (Figure 2a) as compared to the value of absorbance before the impregnation process. The obtained linear dependency (Figure 2b) indicates that process of galvanic displacement can be simply adjusted. However, the values of the slope coefficients of the straight line differ, which suggests that the process of deposition of the two metals on the nickel foam is more complex. Attention should be paid to the possibility of a single exchange between

palladium already deposited on the nickel foam and Pt(IV) ions. This, in consequence, may lead to the formation of bimetallic structures that will affect the efficiency of the catalyzation process. The possible mechanism of galvanic displacement is shown in Figure 3.

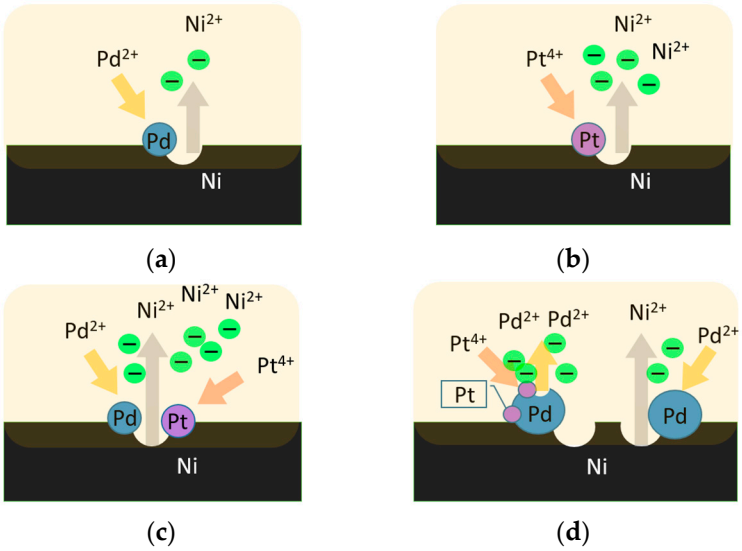

Figure 3. Possible mechanism of galvanic displacement between Ni foam and metal ions: Ni–Pd system (**a**); Ni–Pt system (**b**); Ni–Pd–Pt systems (**c**,**d**).

In the case of a simple system, when only one type of metal ion (0% Pd, 100% Pd) is present in the solution, galvanic displacement runs according to Equations (1) and (2) (see, Figure 3a,b). The addition of the second noble metal ion to the solution might lead to a "double" galvanic displacement according to Equations (1) and (2) (Figure 3c) and additional galvanic displacement between palladium deposited on the Ni surface and platinum ions (Figure 3d). Also, a mixture of both mechanisms is possible, leading to different deposit morphology and compositions. These aspects make a promising tool for the process of catalyst synthesis and surface modification. In order to characterize the obtained materials, SEM/EDS and XRD analysis were performed, and the results are described in Section 2.3.

2.3. Catalyst Characterization

2.3.1. SEM/EDS Analysis of the Catalyst

Before impregnation process Ni foam was analyzed using Scanning Electron Microscopy. Obtained results are shown in Figure S1, Supplementary Materials. As expected, the nickel foam exhibits a typical spatial architecture (Supplementary Materials, Figure S1a,b). Higher magnifications reveal grain structures and boundaries (see, Supplementary Materials, Figure S1c,d). In summary, the three-dimensional structure of the nickel foam provides an ideal substrate for depositing particles of platinum-group metals. It is worth noting that the foam's open structure creates quite large spaces that will not block the reaction products in any way, as may be the case in materials characterized by very high porosity (e.g., carbon-based materials). After Ni foam impregnation in different solutions, the ready-to-use catalysts were obtained. These catalysts were analyzed using SEM at different magnifications in order to characterize the surface morphology and composition. The obtained results are shown in Figure 4.

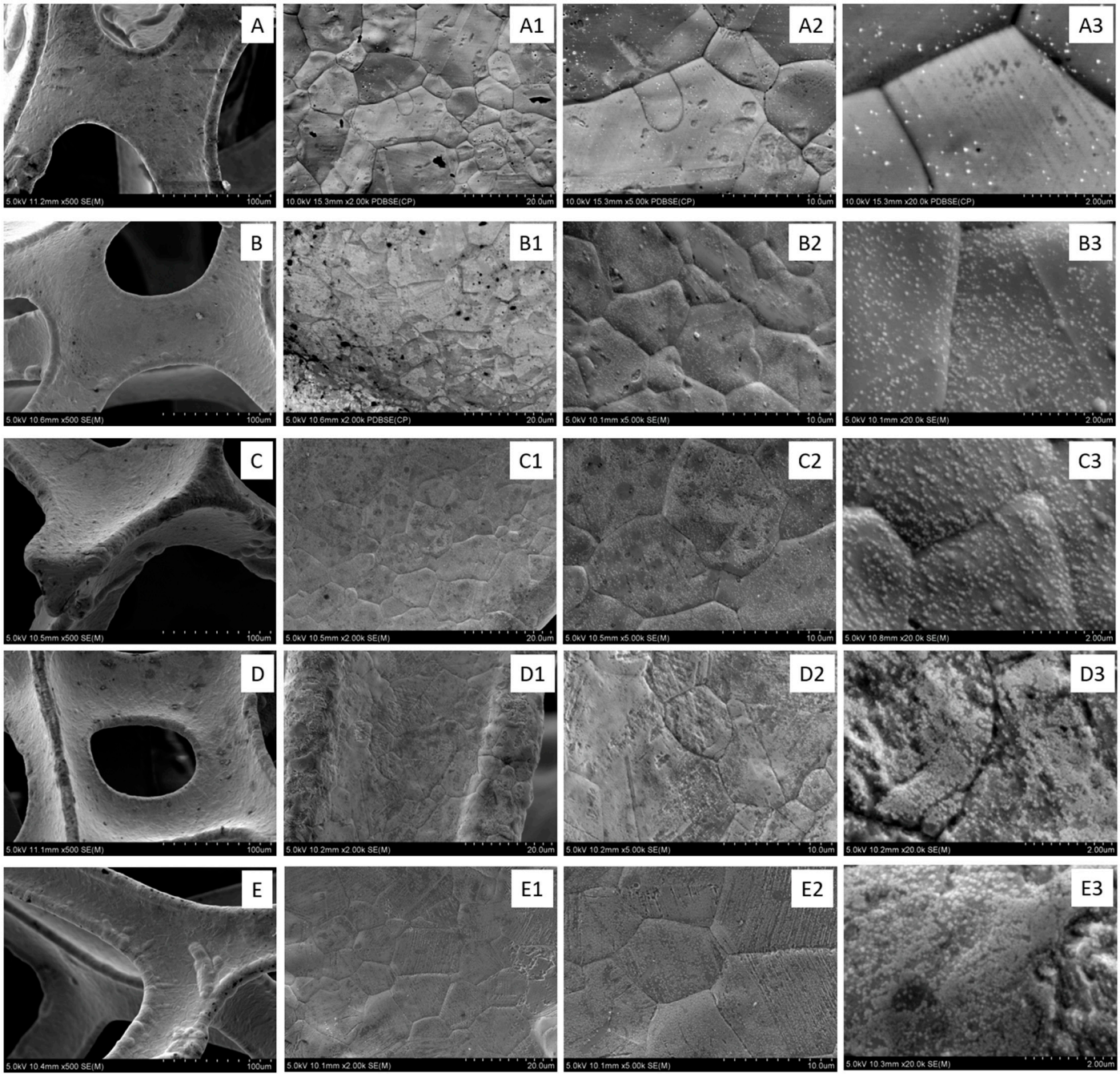

Figure 4. SEM analysis of modified Ni foam: Pd0Pt1.0@Ni (**A**–**A3**); Pd0.25Pt0.75@Ni (**B**–**B3**); Pd0.5Pt0.5@Ni (**C**–**C3**); Pd0.75Pt0.25 (**D**–**D3**); Pd1.0Pt0 (**E**–**E3**). Scale given in micrometers.

The data indicate that the surface morphology of the Ni foam changed after the impregnation process. Depending on the solution's composition, the Ni surface was modified with 50–100 nm particles containing noble metals (Figure 4) at varying coverage levels. As the palladium concentration in the solution increased, nearly complete surface coverage with palladium particles was observed, with the highest coverage in the sample containing 100% Pd (Figure 4E–E3). Catalysts with both metals (Pd0.25Pt0.75@Ni and Pd0.5Pt0.5@Ni) showed the coexistence of two fractions different in size (see, Supplementary Materials, Figure S2).

To confirm the deposition of Pd and Pt on Ni substrate, EDS analysis was carried out. The obtained results are shown in Supplementary Materials, Figure S3 and Table S2. Figure S3 (Supplementary Materials) shows the results of a standardless EDS analysis of

Ni samples covered with Pd and Pt nanoparticles. The analysis confirms the presence of Pt and Pd elements within the examined areas. The EDS qualitative results indicate significant variations in the elemental composition, primarily due to the sample's irregular topography, non-flat surface, and the increased scattering volume of the matrix due to the small particle size. In order to further confirm catalyst composition, XRD analysis was carried out and the obtained results are described in Section 2.3.2.

2.3.2. XRD Analysis of the Catalysts

XRD analysis was carried out for a blank sample (only Ni foam) and selected catalysts obtained from the solution containing different PGM amounts, i.e., Pd0Pt1.0@Ni, Pd0.5Pt0.5@Ni, and Pd1.0Pt0@Ni. The obtained XRD patterns for these materials, in the range of 20–80 degrees, are shown in Figure 5.

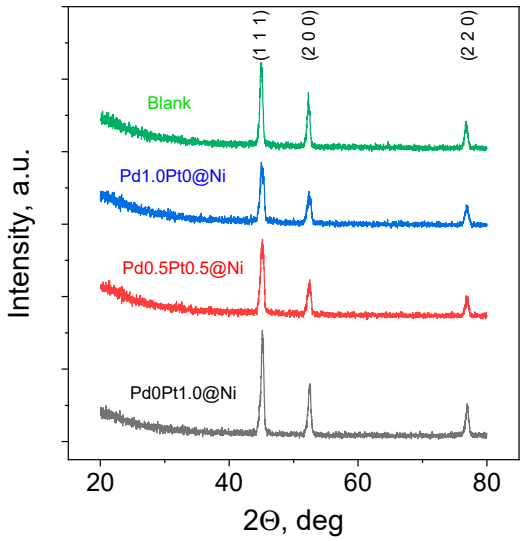

Figure 5. XRD patterns registered for blank and selected catalysts obtained from the solution containing different PGM compositions (Pd0Pt1.0@Ni, Pd0.5Pt0.5@Ni, and Pd1.0Pt0@Ni), at different angle range: 20–80 degrees.

As it can be seen in Figure 5, XRD pattern registered for the blank (only Ni foam) contains three peaks close to that obtained for similar materials [26], i.e., about 45, 52, and 76 degrees (Table 1). The XRD patterns for the synthesized catalysts are similar to that obtained for the blank (Figure 5).

Table 1. Comparison of XRD peak locations for foam used in experiments (blank) and literature data.

Catalyst	2Θ, deg	Compound	Ref.
Ni foam	44.5 51.86 76.39	Ni	[27]
Blank	44.99 52.29 76.94	Ni	This work

All detected peaks come from Ni (1 1 1), (2 0 0), and (2 2 0) planes [27]. Taking into account the character of the catalysts and trace amount of palladium and platinum deposited on Ni foam, the XRD signal coming from these noble metals is very weak and is not detectable in these samples. A similar observation was reported in the literature [23,28,29].

2.4. Catalyst Performance for Hydrogen/Oxygen Evolution Reaction

The modification of the Ni surface with varying amounts of Pd and Pt ions in solution significantly increases the catalytic activity of the samples. Figure 6a presents the cathodic part of the cyclic voltammetry (CV) scans in 1 M NaOH solution, performed in the potential range down to −0.35 V. At this potential, the recorded currents related to hydrogen evolution for various Pd–Pt ratios on Ni foam are as follows: Pd0Pt1.0@Ni −174 mA, Pd1.0Pt0@Ni −225 mA, Pd0.25Pt0.75@Ni −227 mA, Pd0.5Pt0.5@Ni −242 mA, and Pd0.75Pt0.25@Ni −298 mA. This increase in current can be attributed to the gradual enlargement of the surface area and the increase in the number of active sites, where the overpotential for the reduction reaction is lower. A similar effect was previously observed for Co-nanoconical and Ni porous nanostructures decorated with Pd via a galvanic displacement method [30].

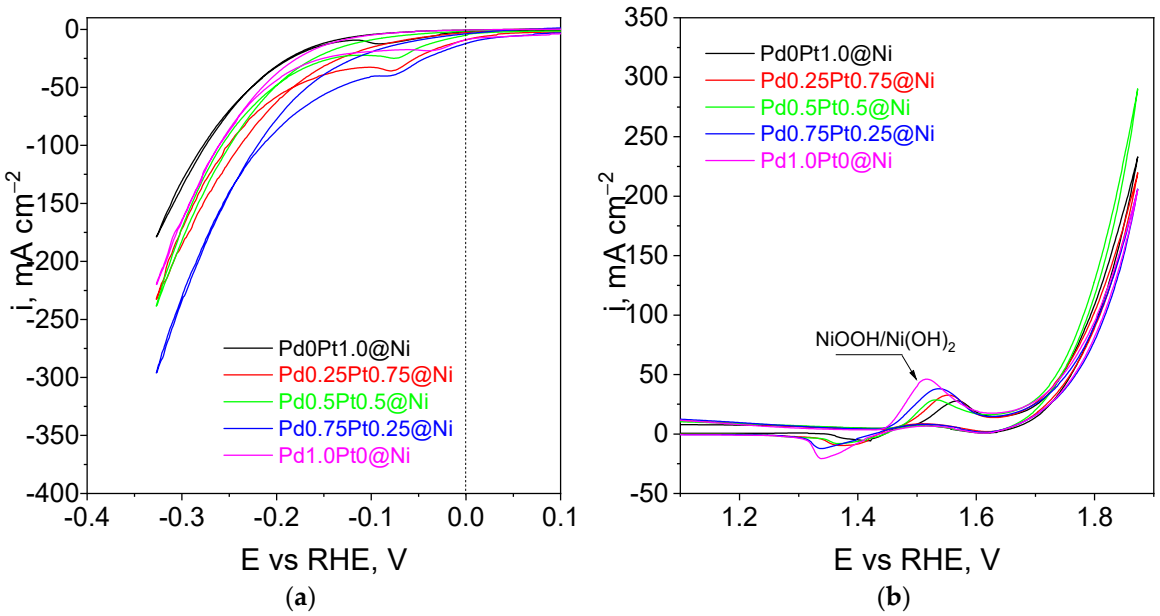

Figure 6. Cyclic voltammetry scans registered in 1 M NaOH solution for Ni foams modified by Pt, Pd, and Pt-Pd with different ion ratios. Cathodic part of CV scan with hydrogen evolution reaction (**a**); anodic part of CV scan with oxygen evolution reaction (**b**).

Figure 6b shows the anodic part of the CV scans, which illustrates the oxygen evolution reaction (OER) in alkaline solution. A first anodic peak appears at approximately 1.35 V, corresponding to the formation of a nickel oxide layer on the electrode surface [31]. The intensity of this peak varies depending on the applied mixture of Pd and Pt ions [32]. However, differences in intensity may depend on the degree of platinum and palladium coverage. Notably, the highest degree of coverage was observed in the peak for the Pd0.5Pt0.5@Ni sample, which correlates with the highest current intensity recorded at 1.9 V. Overall, these CV results indicate that modifying porous nickel structures with even trace amounts of noble metals, obtained from waste solutions, leads to significant improvements in catalytic activity for both hydrogen and oxygen evolution reactions. To further quantify the hydrogen evolution reaction (HER) performance, we evaluated catalytic activity at current densities of -20 mA·cm^{-2} and -100 mA·cm^{-2}. We deliberately avoided -10 mA·cm^{-2} because that current density occurs before the theoretical onset of hydrogen evolution (primarily involving double-layer charging). In these tests, the negative potentials at -20 and -100 mA·cm^{-2} were recorded for each sample. The catalyst without palladium, i.e., Pd0Pt1.0@Ni, reached -0.1815 V at -20 mA·cm^{-2} and -0.2787 V at -100 mA·cm^{-2}, while Pd-containing samples generally exhibited more favorable (i.e., less

negative) potentials at both current densities. In another set of experiments, we compared catalyst performance at fixed overpotentials of −100 and −250 mV. For each sample, we measured the resulting current densities. The presence of Pd substantially enhanced the current density at both overpotentials, with the Pd0.75Pt0.25@Ni sample in particular showing the highest current density at −100 and −250 mV.

The Tafel slopes were determined in the linear current range of −10 to −100 mA·cm^{-2}. Pd0Pt1.0@Ni displayed a Tafel slope of about 137.9 mV·dec^{-1}, while the Pd-decorated foams exhibited lower slopes (ranging from ~120.9 to ~132.5 mV·dec^{-1}), consistent with improved kinetics for hydrogen evolution. For the OER, we found that the NiOOH/Ni(OH)$_2$ redox couple strongly overlaps with lower-current-density regions (+10 or +20 mA·cm^{-2}), complicating an accurate overpotential assessment in that zone. Consequently, +100 mA·cm^{-2} was used as a benchmark. Again, introduction of Pd generally shifted the potential for OER at +100 mA·cm^{-2}, with the Pd0.5Pt0.5@Ni sample showing one of the more favorable values (1.772 V). The HER performance at −100 mA·cm^{-2} with selected literature data is summarized in Table 2.

Table 2. Comparison of HER overpotentials and Tafel slopes with literature data.

Catalyst	Overpotential (@−100 mA·cm^{-2})	Tafel Slope (mV·dec^{-1})	Ref.
Pd0Pt1.0@Ni	−0.2787 V	137.9	This work
Pd0.25Pt0.75@Ni	−0.2539 V	132.5	
Pd0.5Pt0.5@Ni	−0.2498 V	125.2	
Pd0.75Pt0.25@Ni	−0.2220 V	120.9	
Pd1.0Pt0@Ni	−0.2630 V	123.0	
Ni foam	−0.444 V	~130	[30]
Pt/C on GC	not reported	38	[30]
Pt/C	−0.235 V	34	[31]
NiPt	−0.180 V	30	
NiCoPt	−0.150 V	28	

As shown in Table 2, our Pd-modified Ni foam exhibits significantly improved HER activity compared to bare Ni foam (both our own control and that reported in [30]). The overpotential at −100 mA·cm^{-2} is notably lower for the decorated samples, highlighting the beneficial effect of a highly diluted noble metal deposition on the Ni foam framework. While commercial Pt/C and NiCoPt composites can offer lower overpotentials and Tafel slopes, our approach demonstrates that even small amounts of noble metal can substantially boost Ni foam's catalytic performance. The resulting material is both active and durable, making it suitable for various chemical and electrochemical reactions.

Additionally, for the most efficient electrocatalysts, i.e., Pd0.75Pt0.25@Ni and Pd0.5Pt0.5@Ni, the stability tests have been performed. The chronopotentiometric tests for HER and OER in NaOH solution under current conditions of 80 mA for a time of 3600 s were applied. The obtained results are included in Supplementary Materials as a Figure S4a (HER) and Figure S4b (OER). Considering the sample's porous nature and application into a glassy-carbon electrode, the registered potential values are strongly oscillating. This effect is related to forming and accumulating hydrogen/oxygen bubbles inside the porous structure. Moreover, the bubbles are coalescent in time, which can be related to the sharp and significant drops of the registered potential. For the porous Ni substrate, the registered potential value fluctuated enormously. For the first 1200 s, the value oscillated around −0.45 V, dropping to −0.55V and remaining constant. Samples were also tested after Ni foam modification, e.g., Pd0.75Pt0.25@Ni, which exhibits the highest catalytic activity in linear voltammetry scans. Application of an exact current

density of −80 mA allows registering the potential −0.30 V, which was very stable and did not change during the 1 h test. It should be noted that the oscillations and potential drops are significantly smaller and can be related to the state of the surface (formed Pd/Pt nanoparticles), where formed hydrogen bubbles were released much faster than Ni porous substrate. Regarding the oxygen evolution reaction tests, the selected samples were the porous Ni substrate and Pd0.5Pt0.5@Ni sample. It can be seen in both cases that in the first 300 s, the potential value is gradually increasing, and it is related to the formation of the $Ni(OH)_2$ electroactive layer on the electrode surface, which is taking part in the oxygen evolution reaction. This process was much faster for porous Ni than for the Pd-Pt modified one because noble nanoparticles cover the surface. Further, the anodic polarization of the Ni electrode oscillates around the value +2.3 V with some drops related to the departure of formed oxygen bubbles. After 25 min, the course of the line was linear and smooth, and stabilized at a potential value between +2.19 and +2.22 V. The oxygen evolution reaction range stabilization for the noble-metals-modified sample was much faster than for the previously described sample. The registered value was significantly lower (+2.10 V) and increased only by 0.02 V after 50 min. Taking into consideration all presented results, we confirmed higher catalytic activity and good stability in the tested reactions compared to the non-modified Ni porous sample.

2.5. Catalyst Performance for Methyl Orange Removal from Aqueous Solution

2.5.1. Process of Methyl Orange Degradation Using Ascorbic Acid

The process of methyl orange (MO) degradation using ascorbic acid was studied in our previous work [32]. In this study, we used a lower amount of ascorbic acid (0.01 g in 4 mL of MO solution), but still a high enough amount to forward the process of azo dye degradation without the risk of forming reversible intermediates. The addition of ascorbic acid to the MO solution caused a change in pH from about 5 to about 2. This pH change results in a change in the solution color from orange to red, and a share of azo dyes forms [33]. The change in color of the MO solution is associated with the change in the UV-Vis spectrum and shift in the peak position from 466 nm to 504 nm (Figure 7). The spectrum at 272 nm is overlapped by a spectrum characteristic of ascorbic acid, for which the maximum is located at 262 nm [25].

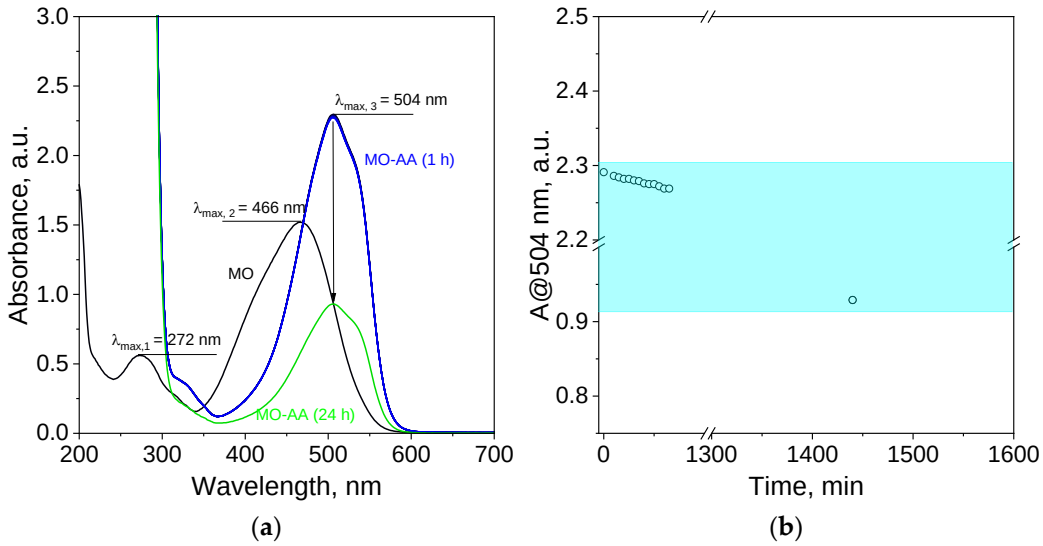

Figure 7. The UV-Vis spectra for the solution containing a mixture of methyl orange (MO) and ascorbic acid (AA) after 1 and 24 h (**a**); fragment of kinetic trace registered at 504 nm and obtained from spectrophotometric study (**b**). Conditions: $C_{0,MO} = 5 \times 10^{-5}$ M, m_{AA} = 0.025 g, T = 20 °C, V = 4 mL, dimension of catalysts 1 cm × 1 cm.

After mixing the ascorbic acid and methyl orange, a slow decrease in absorbance value at 504 nm was registered. The fragment of the kinetic curve is presented in Figure 7b, and confirms that under the selected reaction conditions the process of azo dye degradation is slow. In order to enhance this process, we decided to add the selected Pd0Pt1.0@Ni, Pd0.5Pt0.5@Ni, and Pd1.0Pt0@Ni catalysts to the solution containing azo dye and ascorbic acid. Catalytic tests were also performed for pure Ni foam (blank). The obtained results are shown in the next Sections 2.5.2 and 2.5.3.

2.5.2. Process of Methyl Orange Degradation Using Ascorbic Acid and in the Presence of Catalysts—Long-Term Removal

The process of MO degradation using ascorbic acid was carried out in the presence of selected catalyst compositions. It was observed that the process runs faster but still takes 20 h to be completed; it accelerates by two times compared to the sample without catalyst. Thus, we decided to modify our system with the addition of small amount of hydrogen peroxide to the catalyzed solution. It is known that H_2O_2 takes part in the process of oxidative dye degradation under UV exposure [34–36], as well as using the Fenton system [37–39]. The addition of hydrogen peroxide to the solution containing the azo dye and the catalyst significantly accelerated the process, making spectrophotometric monitoring of dye degradation difficult. Therefore, the surface area of the catalysts was reduced by four times comparing to previous catalytic tests. The obtained results are described in detail in Section 2.5.3.

2.5.3. The Methyl Orange Degradation in the Presence of Catalyst and H_2O_2—Short-Term Removal

The process of methyl orange degradation using a modified Fenton reaction (no Fe(II) was added, ascorbic acid is treated as a source of electron in the process) in the presence of catalysts (1/4 part) was carried out. For comparison, we studied also the process of MO degradation in the system without catalysts and in the presence of an unmodified Ni foam. For this purpose, one drop of hydrogen peroxide was added to solutions containing methyl orange, ascorbic acid, and the catalyst. Next, the process of MO degradation was followed spectrophotometrically up to its end (see Figure 8 and Supplementary Materials, Figure S5).

Comparing spectra obtained for the process without and with a catalyst addition (Figure 8a,b), we observed an acceleration of the MO degradation process. After 10 min, the efficiency of the degradation process is 9.2% (efficiency (E) is calculated from the equation $E = 100\% \cdot (A_0 - A_{t=10min})/A_0$, where A_0—absorbance value at t = 0 min, $A_{t=10min}$—absorbance value at t = 10 min) (Figure 8a), while in the case of using a catalyst, after the same time it reaches 73% (Figure 8b). Based on the obtained spectra, kinetic curves were drawn (see, Figure 8c) and the fitted equation (Boltzmann) has been selected. Detailed information about fitting parameters in the Boltzmann equation was gathered in Supplementary Materials, Table S3. The addition of H_2O_2 triggers the process of MO removal, due to Fenton's mechanism. The time was shortened from 20 h to 15 min depending on the catalyst composition (even when the catalyst dimension was reduced by four times). The registered spectra evolution (Figure 8a,b, Supplementary Materials, Figure S5) and kinetic curves determined from them, shown in Figure 8c, indicate that the process runs in the order Pd1.0Pt0@Ni > Pd0Pt1.0@Ni > Pd0.5Pt0.5@Ni > Ni foam (blank) > no catalyst. The time needed for MO degradation at the level of 50% its initial amount increases in the order $t_1 > t_2 > t_3 > t_4 > t_5$, see Figure S5, Table S3. This implies that the addition of a noble metal to the catalyst's composition inhibits the process of azo-dye degradation. It is interesting that the catalyst containing a mixture of palladium and platinum is slower than the catalyst containing pure metals. This can be explained by the surface morphology and

the mechanism of galvanic displacement which is more complex (see Figure 3 and results from SEM analysis, Figure 5).

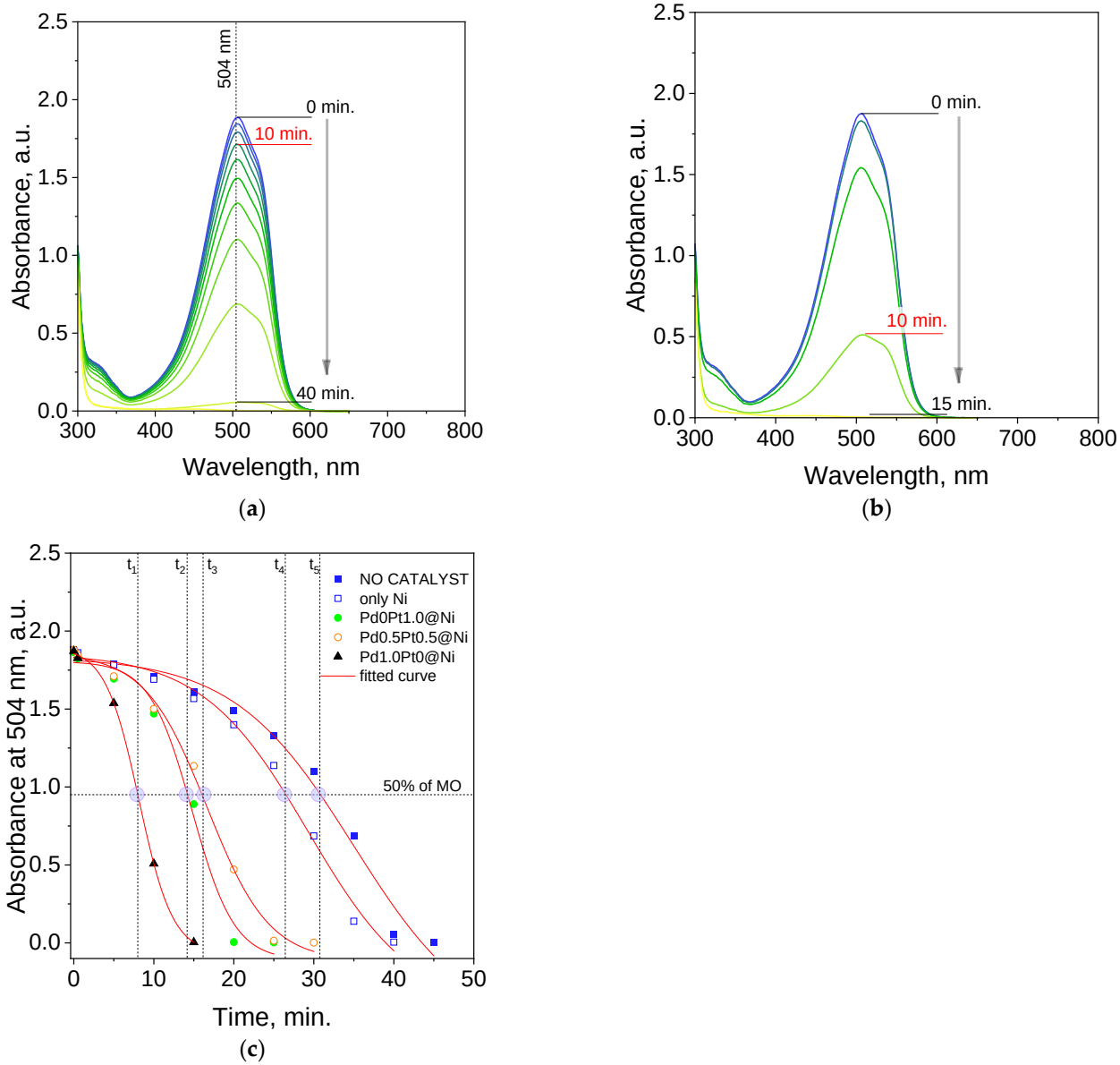

Figure 8. UV-Vis spectra evolution for solutions containing a mixture of MO, ascorbic acid, and H_2O_2 in the presence of (**a**) no catalyst; (**b**) Pd1.0Pt0@Ni. Kinetic data registered at 504 nm for all studied systems: without catalyst, with Ni foam (blank), and catalyst with different compositions: Pd0Pt1.0@Ni, Pd0.5Pt0.5@Ni, and Pd1.0Pt0@Ni (**c**) and kinetic curves fitted to the experimental data (Boltzmann's equation). Conditions: 3 mL MO 5×10^{-5} M, m_{AA} = 0.0187 g, 1 drop (50 µL) of H_2O_2, total time 45 min, interval 5 min, T = 20 °C, mixing rate 1000 RPM. Of note: $t_{1–5}$—time in Boltzmann equation at which 50% of MO is degraded (**c**), purple circle on the graph was used only as marker to highlight crossing lines.

3. Materials and Methods

3.1. Reagents

PGM base solutions. As a palladium and platinum precursors, base solutions of 0.093 M H_2PdCl_4 and 0.076 M H_2PtCl_6 obtained from pure metals (Mennica Państwowa, 99.99%, Warsaw, Poland), according to the procedure described in the literature [40,41], were used. Depending on the solution composition, different volumes of base solution

containing of Pd(II) and Pt(IV) ions were dissolved in 0.1 M HCl (Avantor Performance Materials Poland, Gliwice, Poland) in a volumetric flask (10 mL).

Ascorbic acid (AA). Ascorbic acid (p.a., Avantor Performance Materials Poland, Gliwice, Poland) was used as received in the form of powder.

Hydrogen peroxide (H_2O_2). Commercially available 3% solution of H_2O_2 from the pharmacy was acquired. During experiments, 50 μL of H_2O_2 solution was added to the vial containing MO solution, or MO with ascorbic acid addition.

Ni foam. Commercially available Ni foam was delivered from Xiamen Lith Machine Limited, Xiamen City, China. Porosity was 97%, purity was ≥99.8%, and areal density was 350 ± 20 g/m^2. Then, the sponge was cut into smaller pieces with dimensions 1 cm × 1 cm. Such prepared samples were cleaned in 0.1 M HCl under ultrasonic conditions for 10 min to remove possible oxides from the foam surface. Next, samples were cleaned in deionized water and ethanol and dried. Ready catalysts were cut into smaller pieces with a mass equal to 0.0082 g.

3.2. Methods of Analysis

UV-Vis spectrophotometry (Shimadzu, Kyoto, Japan). A UV-Vis spectrophotometer (190–900 nm) was used for determination of spectra coming from reagents for spectra evolution registration. For this purpose, a solution containing the samples was introduced to a quartz cuvette (Hellma GmbH & Co. KG, Müllheim, Germany, path length 1 cm) and thermostatic measurement cell. At all points, 0.1 M HCl was used as a reference solution.

X-Ray Diffraction (XRD) analysis. The XRD method (Rigaku MiniFlex II) analyzed the phase composition using a copper tube (λ = 1.54059). Experiments were carried out in a range of 2-theta values between 20 and 80 degrees with a scan rate of 0.5 deg/min. The obtained diffractograms were compared with data in the literature.

Scanning Electron Microscope (SEM) analysis. The distribution and morphology of the deposited materials were characterized by an ultra-high-resolution Hitachi SU-70 FEG scanning electron microscope (Hitachi, Tokyo, Japan). SEM imaging was performed on Ni foam substrate and the as-deposited samples, utilizing secondary electron (SE) and back-scattered electron (BSE) modes. The chemical composition of deposited Pt and Pd products was analyzed by Energy-Dispersive X-ray Spectroscopy (EDS).

Catalytic tests. The electrochemical performance of obtained materials were tested by a Biologic SP-200 potentiostat controlled by a PC with EC-Lab dedicated software V10.37. The catalytic performance of the modified Ni foams was estimated using cyclic voltammetry. All measurements were carried out in a 1 M NaOH solution. The measured potentials for LSV experiments were converted to the reversible hydrogen electrode (RHE) scale using the Nernst equation:

$$E_{RHE} = E_{Hg/Hg2Cl2} + 0.059pH + E^{\circ}_{Hg/Hg2Cl2} \quad (3)$$

where E_{RHE} is the converted potential vs. RHE, $E_{Hg/Hg2Cl2}$ is the experimentally measured potential against Hg/Hg_2Cl_2 reference electrode, and $E^{\circ}_{Hg/Hg2Cl2}$ is the standard potential of Hg/Hg_2Cl_2 at 25 °C (0.245 V).

Each sample was immersed in NaOH solution immediately after the modification process and held in the solution for 5 min to stabilize the open-circuit potential (OCP) value, which served as the starting point for the CV measurements. The sodium hydroxide solution before experiments was purged with argon gas to remove dissolved oxygen, which could interfere with the results. The current values were calculated, the geometrical surface of the samples was 0.25 cm^2, and each porous sample weighed 0.0082 g. Cyclic voltammetry scans were performed at a scan rate of 50 mV/s with a non-stirred electrolyte.

Stability test. The stability tests were performed for selected catalysts by application of -80 mAcm^{-2} in terms of hydrogen evolution and 80 mAcm^{-2} for oxygen evolution reaction. The measurements were carried out for 1 h. The samples were normalized by their weight, and it was assumed that the working electrode surface was similar.

4. Conclusions

The Waste for Product approach was successfully demonstrated. The process of galvanic displacement and selected experimental conditions allowing for the synthesis of universal catalyst deposited on Ni foam was shown to work both for HER/OER as well as methyl orange degradation. The catalyst efficiency depends on the catalyst morphology and composition. In the case of HER/OER, the presence of palladium and platinum in the catalyst structure revealed improved electrocatalytic performance compared to pure metals, indicating a synergistic effect. For the process of methyl degradation, using a catalyst containing palladium nanoparticles deposited on Ni foam is the most efficient. The advantage of the proposed method is its simplicity, short time of catalyst production, and low costs. Moreover, the solution after the impregnation process of Ni foam can be again used up to complete PGM removal from waste solution.

Supplementary Materials: The following supporting information can be downloaded at: https://www.mdpi.com/article/10.3390/catal15020133/s1, Table S1. Detailed information about solution composition used during experiments; Figure S1. SEM analysis Ni sponge before impregnation process at different magnifications (a–d); Figure S2. SEM analysis of catalysts with different compositions: Pd0.25Pt0.75@Ni (a); Pd0.5Pt0.5@Ni (b) and Pd0.75Pt0.25@Ni (c); Figure S3. Results of EDS chemical analysis (a'–e') for performed in the areas marked on SEM image (a–e) of different catalysts: Pd1.0Pt0@Ni (a,a'), Pd0.75Pt0.25@Ni (b,b'), Pd0.5Pt0.5@Ni (c,c'), Pd0.25Pt0.75@Ni (d,d'), Pd0Pt1.0@Ni (e,e'); Table S2. EDS chemical analysis obtained for different catalysts composition; Figure S4. Chronopotentiometric stability tests for HER (a) and OER (b) performed in 1 M NaOH solution. Applied current density: 80 mA·cm^{-2}, time: 3600 s; Figure S5. UV-Vis spectra evolution for solutions containing mixture of MO, ascorbic acid, H_2O_2 in the presence of Pd0.5Pt0.5@Ni (a); Pd0Pt1.0@Ni (b) and Ni–sponge (c). Conditions: 3 mL MO 5×10^{-5} M, mAA = 0.0187 g, 1 drop (50 µL) of H_2O_2, total time 45 min, interval 5 min, T = 20 °C, mixing rate 1000 RPM; Table S3. Parameters in Boltzmann equations fitted to kinetic data during process of MO degradation.

Author Contributions: Conceptualization, M.L.-B. and D.K.; methodology, M.L.-B.; formal analysis, M.L.-B., D.K. and A.K.; investigation, J.D., A.K. and D.K.; writing—original draft preparation, M.L.-B., D.K., A.P. and A.K.; writing—review and editing, M.L.-B.; visualization, M.L.-B. and D.K.; project administration, M.L.-B. All authors have read and agreed to the published version of the manuscript.

Funding: This research was funded by AGH University under the Rector's Grant, grant no. 54/GRANT/2024.

Institutional Review Board Statement: Not applicable.

Informed Consent Statement: Not applicable.

Data Availability Statement: Data are contained within the article and Supplementary Materials.

Conflicts of Interest: The authors declare no conflicts of interest.

References

1. Salonen, L.M.; Petrovykh, D.Y.; Kolen'ko, Y.V. Sustainable catalysts for water electrolysis: Selected strategies for reduction and replacement of platinum-group metals. *Mater. Today Sustain.* **2021**, *11–12*, 100060. [CrossRef]
2. Chen, H.; Liang, X.; Liu, Y.; Ai, X.; Asefa, T.; Zou, X. Active Site Engineering in Porous Electrocatalysts. *Adv. Mater.* **2020**, *32*, e2002435. [CrossRef]

3. Sheng, W.; Gasteiger, H.A.; Shao-Horn, Y. Hydrogen Oxidation and Evolution Reaction Kinetics on Platinum: Acid vs Alkaline Electrolytes. *J. Electrochem. Soc.* **2010**, *157*, B1529. [CrossRef]
4. Shah, A.H.; Wan, C.; Huang, Y.; Duan, X. Toward Molecular Level Understandings of Hydrogen Evolution Reaction on Platinum Surface. *J. Phys. Chem. C* **2023**, *127*, 12841–12848. [CrossRef]
5. Tiwari, J.N.; Sultan, S.; Myung, C.W.; Yoon, T.; Li, N.; Ha, M.; Harzandi, A.M.; Park, H.J.; Kim, D.Y.; Chandrasekaran, S.S.; et al. Multicomponent electrocatalyst with ultralow Pt loading and high hydrogen evolution activity. *Nat. Energy* **2018**, *3*, 773–782. [CrossRef]
6. Hou, J.; Yang, M.; Ke, C.; Wei, G.; Priest, C.; Qiao, Z.; Wu, G.; Zhang, J. Platinum-group-metal catalysts for proton exchange membrane fuel cells: From catalyst design to electrode structure optimization. *EnergyChem* **2020**, *2*, 100023. [CrossRef]
7. Spiegel, R.J. Platinum and fuel cells. *Transp. Res. Part D Transp. Environ.* **2004**, *9*, 357–371. [CrossRef]
8. Ren, X.; Wang, Y.; Liu, A.; Zhang, Z.; Lv, Q.; Liu, B. Current progress and performance improvement of Pt/C catalysts for fuel cells. *J. Mater. Chem. A* **2020**, *8*, 24284–24306. [CrossRef]
9. Wang, X.; Zhu, Y.; Vasileff, A.; Jiao, Y.; Chen, S.; Song, L.; Zheng, B.; Zheng, Y.; Qiao, S.-Z. Strain Effect in Bimetallic Electrocatalysts in the Hydrogen Evolution Reaction. *ACS Energy Lett.* **2018**, *3*, 1198–1204. [CrossRef]
10. Yu, W.; Porosoff, M.D.; Chen, J.G. Review of Pt-Based Bimetallic Catalysis: From Model Surfaces to Supported Catalysts. *Chem. Rev.* **2012**, *112*, 5780–5817. [CrossRef]
11. Beletskaya, I.P.; Cheprakov, A.V. The Heck Reaction as a Sharpening Stone of Palladium Catalysis. *Chem. Rev.* **2000**, *100*, 3009–3066. [CrossRef] [PubMed]
12. D'Alterio, M.C.; Casals-Cruañas, È.; Tzouras, N.V.; Talarico, G.; Nolan, S.P.; Poater, A. Mechanistic Aspects of the Palladium-Catalyzed Suzuki-Miyaura Cross-Coupling Reaction. *Chem. Eur. J.* **2021**, *27*, 13481–13493. [CrossRef]
13. Emadi, R.; Bahrami Nekoo, A.; Molaverdi, F.; Khorsandi, Z.; Sheibani, R.; Sadeghi-Aliabadi, H. Applications of palladium-catalyzed C–N cross-coupling reactions in pharmaceutical compounds. *RSC Adv.* **2023**, *13*, 18715–18733. [CrossRef]
14. Doucet, H.; Hierso, J.-C. Palladium-Based Catalytic Systems for the Synthesis of Conjugated Enynes by Sonogashira Reactions and Related Alkynylations. *Angew. Chem. Int. Ed.* **2007**, *46*, 834–871. [CrossRef] [PubMed]
15. Gazvoda, M.; Virant, M.; Pinter, B.; Košmrlj, J. Mechanism of copper-free Sonogashira reaction operates through palladium-palladium transmetallation. *Nat. Commun.* **2018**, *9*, 4814. [CrossRef] [PubMed]
16. Pianowska, K.; Kluczka, J.; Benke, G.; Goc, K.; Malarz, J.; Ochmański, M.; Leszczyńska-Sejda, K. Solvent Extraction as a Method of Recovery and Separation of Platinum Group Metals. *Materials* **2023**, *16*, 4681. [CrossRef] [PubMed]
17. Zheng, H.; Ding, Y.; Wen, Q.; Liu, B.; Zhang, S. Separation and purification of platinum group metals from aqueous solution: Recent developments and industrial applications. *Resour. Conserv. Recycl.* **2021**, *167*, 105417. [CrossRef]
18. Kalavrouziotis, I.K.; Koukoulakis, P.H. The Environmental Impact of the Platinum Group Elements (Pt, Pd, Rh) Emitted by the Automobile Catalyst Converters. *Water Air Soil Pollut.* **2009**, *196*, 393–402. [CrossRef]
19. Gagnon, Z.E.; Newkirk, C.; Hicks, S. Impact of Platinum Group Metals on the Environment: A Toxicological, Genotoxic and Analytical Chemistry Study. *J. Environ. Sci. Health Part A* **2006**, *41*, 397–414. [CrossRef]
20. Ravindra, K.; Bencs, L.; Van Grieken, R. Platinum group elements in the environment and their health risk. *Sci. Total Environ.* **2004**, *318*, 1–43. [CrossRef]
21. Pach, A.; Zaryczny, A.; Michałek, T.; Kamiński, H.; Kutyła, D.; Tokarski, T.; Chat-Wilk, K.; Hessel, V.; Luty-Błocho, M. One-Step Synthesis of Pt–Pd@ACF Catalyst in the Microreactor System for the Hydrogen Evolution Reaction. *Ind. Eng. Chem. Res.* **2024**, *63*, 7018–7030. [CrossRef]
22. Luty-Błocho, M.; Pach, A.; Kutyła, D.; Kula, A.; Małecki, S.; Jeleń, P.; Hessel, V. Waste for Product—Synthesis and Electrocatalytic Properties of Palladium Nanopyramid Layer Enriched with PtNPs. *Materials* **2024**, *17*, 4165. [CrossRef]
23. Wang, D.; Chen, Y.; Yao, B.; Meng, T.; Xu, Y.; Jiao, D.; Xing, Z.; Yang, X. Microdynamic modulation through Pt–O–Ni proton and electron "superhighway" for pH-universal hydrogen evolution. *J. Energy Chem.* **2025**, *101*, 808–815. [CrossRef]
24. Wojnicki, M.; Podborska, A. The Mechanism of Redox Reaction between Palladium(II) Complex Ions and Potassium Formate in Acidic Aqueous Solution. *Arch. Metall. Mater.* **2017**, *62*, 737–745. [CrossRef]
25. Luty-Błocho, M.; Szot, A.; Hessel, V.; Fitzner, K. The Kinetics of the Redox Reaction of Platinum(IV) Ions with Ascorbic Acid in the Presence of Oxygen. *Materials* **2023**, *16*, 4630. [CrossRef]
26. Kutyła, D.; Nakajima, K.; Fukumoto, M.; Wojnicki, M.; Kołczyk-Siedlecka, K. Electrocatalytic Performance of Ethanol Oxidation on Ni and Ni/Pd Surface-Decorated Porous Structures Obtained by Molten Salts Deposition/Dissolution of Al-Ni Alloys. *Int. J. Mol. Sci.* **2023**, *24*, 3836. [CrossRef] [PubMed]
27. Richardson, J.T.; Scates, R.; Twigg, M.V. X-ray diffraction study of nickel oxide reduction by hydrogen. *Appl. Catal. A Gen.* **2003**, *246*, 137–150. [CrossRef]
28. Song, C.; Cao, L.; Li, B.; Huang, X.; Ye, K.; Zhu, K.; Cao, D.; Cheng, K.; Wang, G. Highly efficient palladium nanoparticles decorated reduced graphene oxide sheets supported on nickel foam for hydrogen peroxide electroreduction. *Appl. Surf. Sci.* **2017**, *426*, 1046–1054. [CrossRef]

29. Holder, C.F.; Schaak, R.E. Tutorial on Powder X-ray Diffraction for Characterizing Nanoscale Materials. *ACS Nano* **2019**, *13*, 7359–7365. [CrossRef] [PubMed]
30. Hu, X.; Tian, X.; Lin, Y.-W.; Wang, Z. Nickel foam and stainless steel mesh as electrocatalysts for hydrogen evolution reaction, oxygen evolution reaction and overall water splitting in alkaline media. *RSC Adv.* **2019**, *9*, 31563–31571. [CrossRef]
31. Zhao, S.; Li, R.; Lv, Y.; Ye, H. Self-supported urchin-like NiCoPt/nickel foam as an efficient electrocatalyst for hydrogen evolution reaction in alkaline media. *Chem. Phys. Lett.* **2024**, *834*, 140973. [CrossRef]
32. Pach, A.; Zaryczny, A.; Podborska, A.; Luty-Błocho, M. The Role of Ascorbic Acid in the Process of Azo Dye Degradation in Aqueous Solution. *Molecules* **2024**, *29*, 3659. [CrossRef] [PubMed]
33. Podborska, A.; Luty-Błocho, M. Molecular structure of methyl orange and its role in the process of [Pd(Azo)] compound and MOF formation. *J. Mol. Struct.* **2023**, *1273*, 134312. [CrossRef]
34. Colonna, G.M.; Caronna, T.; Marcandalli, B. Oxidative degradation of dyes by ultraviolet radiation in the presence of hydrogen peroxide. *Dyes Pigments* **1999**, *41*, 211–220. [CrossRef]
35. Ince, N.H. "Critical" effect of hydrogen peroxide in photochemical dye degradation. *Water Res.* **1999**, *33*, 1080–1084. [CrossRef]
36. Dhawle, R.; Frontistis, Z.; Mantzavinos, D.; Lianos, P. Production of hydrogen peroxide with a photocatalytic fuel cell and its application to UV/H_2O_2 degradation of dyes. *Chem. Eng. J. Adv.* **2021**, *6*, 100109. [CrossRef]
37. Swaminathan, K.; Sandhya, S.; Carmalin Sophia, A.; Pachhade, K.; Subrahmanyam, Y.V. Decolorization and degradation of H-acid and other dyes using ferrous–hydrogen peroxide system. *Chemosphere* **2003**, *50*, 619–625. [CrossRef]
38. Malik, P.K.; Saha, S.K. Oxidation of direct dyes with hydrogen peroxide using ferrous ion as catalyst. *Sep. Purif. Technol.* **2003**, *31*, 241–250. [CrossRef]
39. Wang, D.; Qiu, S.; Wang, M.; Pan, S.; Ma, H.; Zou, J. Spectrophotometric determination of hydrogen peroxide in water by oxidative decolorization of azo dyes using Fenton system. *Spectrochim. Acta Part A Mol. Biomol. Spectrosc.* **2019**, *221*, 117138. [CrossRef] [PubMed]
40. Luty-Błocho, M.; Wojnicki, M.; Włoch, G.; Fitzner, K. Green method for efficient PdNPs deposition on carbon carrier in the microreactor system. *J. Nanopart. Res. Interdiscip. Forum Nanoscale Sci. Technol.* **2018**, *20*, 239. [CrossRef] [PubMed]
41. Luty-Błocho, M. The influence of steric stabilization on process of Au, Pt nanoparticles formation. *Arch. Metall. Mater.* **2019**, *64*, 55–63. [CrossRef]